nature nanotechnology

ARTICLES

https://doi.org/10.1038/s41565-022-01126-z

Atomic-scale friction between single-asperity contacts unveiled through in situ transmission electron microscopy

Xiang Wang[1,3], Zhenyu Liu[1,3], Yang He[1], Susheng Tan[2], Guofeng Wang[1]✉ and Scott X. Mao[1]✉

Friction and wear are detrimental to functionality and reduce the service life of products with mechanical elements. Here, we unveil the atomic-scale friction of a single tungsten asperity in real time through a high-resolution transmission electron microscopy investigation of a nanocontact in countermotion, induced through a piezo actuator. Molecular dynamics simulations provide insights into the sliding pathway of interface atoms and the dynamic strain/stress evolution at the interface. We observe a discrete stick–slip behaviour and an asynchronous process for the accumulation and dissipation of the strain energy together with the non-uniform motion of interface atoms. Our methodology allows for studying in situ atomic-friction phenomena and provides insights into friction phenomena at the atomic scale.

Friction and wear are the major sources of the service failure of devices and unexpected energy dissipation in mechanical applications[1]. Unravelling the underlying friction mechanism at the atomic scale is desired to reduce the energy consumption and extend the devices' service life[2,3]. Atomic force microscopy (AFM)-based technologies have been applied to investigate the atomic friction processes. Atomic stick–slip friction, one typical case manifested by a periodic sawtooth-like oscillation in the lateral force–displacement function, was first observed in the sliding of a tungsten probe on a graphite surface under AFM[4]. Thereafter, similar atomic-friction behaviour has been observed in ceramics[5], metals[6,7] and two-dimensional materials[8]. Numerous atomic-friction mechanisms, especially on the transition between stick–slip and superlubricity, have been proposed through investigating the friction dependence on contact configuration[5,9,10] and the scan conditions[6,7,11]. However, the physical sliding scenario between the contacts and the buried surface/interface deformation during friction are still elusive due to the lack of direct interface observation. In situ experiments, especially transmission electron microscopy (TEM) observation, are thus preferable to directly visualize the actual atomic-friction processes. Pioneer in situ TEM unveiled liquid-like tribological phenomena[12] and the formation and shear deformation of a nanojunction[13,14] between metal surfaces and directly captured shear-induced interlayer sliding in two-dimensional materials[15]. Moreover, the formation and motion of nanosized wear particles[16] and a stress-assisted atom-by-atom wear process[17] were disclosed by in situ TEM observation. Despite progress, visualizing the atomically resolved friction process with a clear-cut interface has not been achieved yet. As a result, the relationship between the friction mechanisms and interface structure has not been fully understood. Recently, an advanced in situ TEM platform with high resolution[18,19] has permitted us to image the interface structure between nanocontacts and further investigate the dynamic atomic-friction processes. Complementarily, molecular dynamics (MD) simulations can render insights into interface dynamics, such as the dynamic evolution of surface morphology[20] and the movement of interacting atoms[21] in atomic friction.

In this article, by designing nanocontacts and performing in situ countermotion driven by piezo actuators between tungsten (W) asperities, the real-time single-asperity atomic friction with explicit interface evolution was successfully visualized under high-resolution TEM (HRTEM). The sliding pathway of interface atoms and the dynamic strain/stress evolution on the interface have been elaborated by atomistic MD simulations. Importantly, by examining the interface structure and the scanning conditions between asperities, the processes underlying the observed unique sliding behaviour and the abnormal interface dynamics have been investigated. This allowed us to obtain a fundamental understanding at the atomic scale of (1) the discrete stick–slip friction and (2) the asynchronous accumulation and dissipation of the strain energy between single-asperity contacts.

Discrete stick–slip friction

To visualize the single-asperity atomic-friction processes, a face-to-face nanocontact and subsequent countermotion were performed between a mobile W tip controlled by the piezo actuator and a stiff W substrate under HRTEM (Fig. 1 and Supplementary Video 1). Detailed procedures are given in Methods. The atomic friction showed typical stick–slip behaviour[4], in that the shear force (friction force) fluctuated periodically with the sliding displacement (Fig. 1a). We found that there exist two distinct slipping events, indicated by Slip1 and Slip2, within one lattice period, suggesting a discrete stick–slip behaviour[22] (Fig. 1a), rather than a consecutive slipping described by the Prandtl–Tomlinson (P–T) model[23] in the cases of sliding on Cu[6] and NaCl surfaces[11]. The sequential friction process indicated by the letters in Fig. 1a is shown in Fig. 1b–f. The flat substrate and tip contacted with each other face-to-face along [1$\bar{1}$0] and a well-arranged interface was presented without the diffusion interference from soft metals[14] (Fig. 1b). The starting point (Fig. 1b) possessed a negative shear force due to the lattice distortion induced by the interplay between asperities[24] or caused by the existence of defects such as vacancies formed after in situ melting[25]. As the tip moved horizontally, the shear force increased gradually

[1]Department of Mechanical Engineering and Materials Science, University of Pittsburgh, Pittsburgh, PA, USA. [2]Petersen Institute of Nanoscience and Engineering, University of Pittsburgh, Pittsburgh, PA, USA. [3]These authors contributed equally: Xiang Wang, Zhenyu Liu. ✉e-mail: guw8@pitt.edu; sxm2@pitt.edu

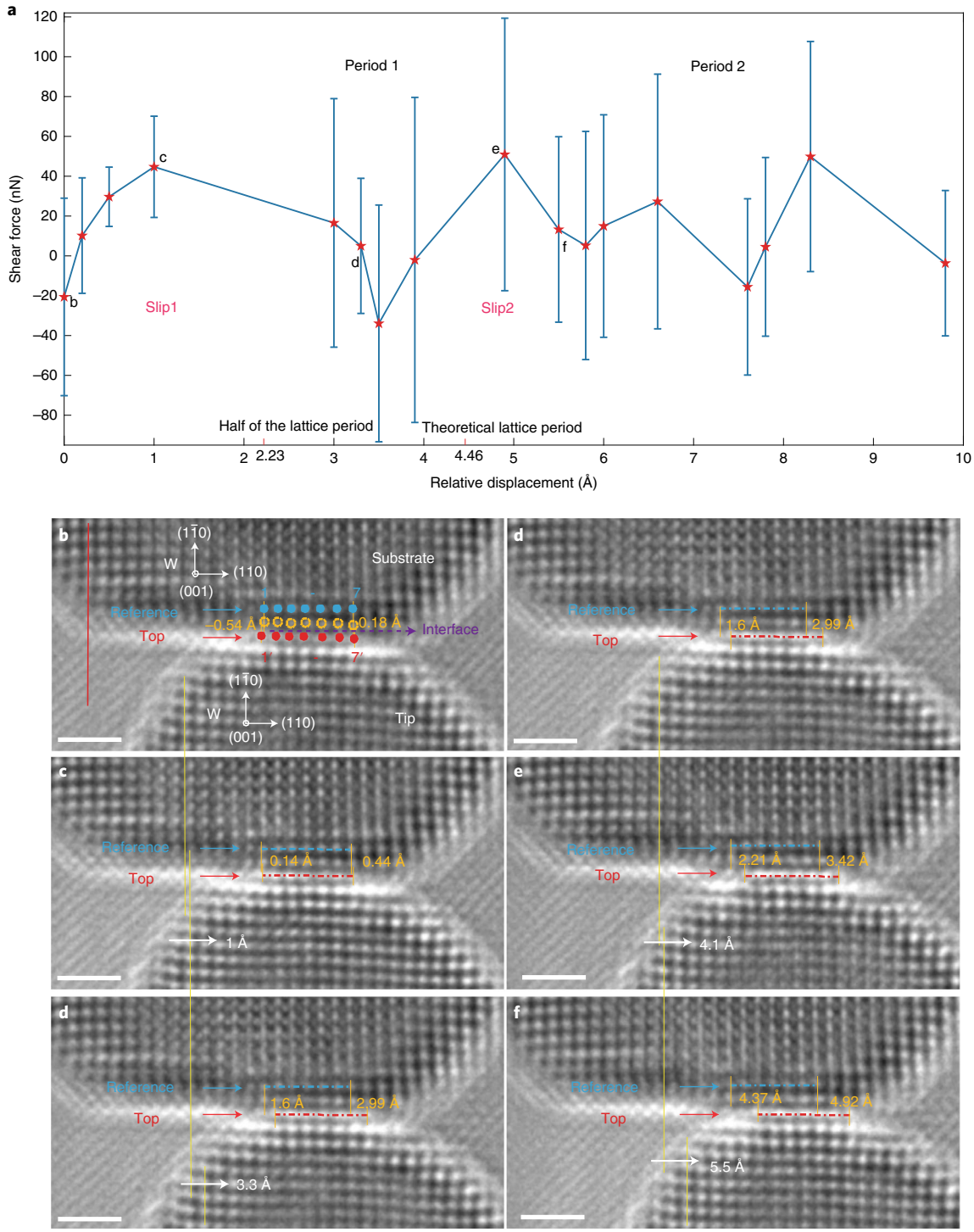

Fig. 1 | In situ atomic observation of stick–slip behaviour between single-tungsten asperity nanocontacts. a, Variation of the shear force with the sliding displacement of the tip. The first and second slippings are indicated by Slip1 and Slip2, respectively and two sliding periods are indicated by Period 1 and Period 2. The error bars represent the standard deviation of the shear force. **b**–**f**, Serial images of the friction process at one period. The theoretical value of lattice spacing along the [110] direction on the $(1\bar{1}0)$ plane is 4.46 Å, indicated in **b**. The relative motion between asperities is indicated by the white arrows. The normal force was controlled by adjusting the asperity separation distance (~2.14 Å, less than the plane spacing of 2.23 Å) and the countermotion was set up along [110] (**b**). The top layer of the tip and the reference layer of the substrate are indicated by the red and blue solid circles (**b**) and the short dotted lines (**c**–**f**), respectively and are numbered 1~7 and 1′~7′. The bottom layer in the substrate is indicated by the broken circles. Two atom columns, indicated by the red and yellow vertical lines in the substrate and tip, respectively, served as the reference coordinates to determine the relative displacement between the asperities. The absolute distance between the reference layer and the interface layer along [110] is indicated by yellow numbers and the relative displacement between the substrate and the tip is indicated by white numbers. Scale bars, 1 nm. Panel **d** is repeated for ease of interpretation.

to reach the first peak (Fig. 1c). Then, Slip1 occurred and the shear force dropped dramatically as the tip had shifted by ~3.3 Å (Fig. 1d). Similar to the first stick–slip, the shear force climbed to the second stick point and subsequently descended after Slip2 (Fig. 1e,f). The total sliding displacement of the tip was ~5.5 Å, close to the lattice spacing along [1$\bar{1}$0]. Period 2 showed an analogous pattern to Period 1. The slipping of the tungsten tip appeared to possibly follow a zigzag route containing two sliding steps within one period[5,26].

Interestingly, we discovered that the movement of the top layer was not synchronous with the sliding of the tip. Two atoms at either end on the top layer (indicated by red circles and numbered 1′ and 7′) were selected to assess the motion of the top layer relative to the substrate, one immovable layer with negligible deformation (atoms indicated by the blue circles and numbered 1 and 7, Fig. 1b). The initial distances between atoms 1 and 1′ and atoms 7 and 7′ were −0.54 and 0.18 Å, respectively along the sliding direction (Fig. 1b) and this increased to 0.14 and 0.44 Å (Fig. 1c). Relative displacements for both sides of the top layer with respect to the substrate were only 0.68 and 0.26 Å, smaller than the relative sliding displacement (1.0 Å) of the whole tip, implying a hysteretic motion of the top layer compared to the whole tip. The subsequent sliding process exhibited similar phenomena indicated by the yellow and white numbers in Fig. 1d–f. These results showed that the displacement within the tip was progressively transmitted from the bottom (drive end) to the top, consistent with the assumption treating the nanoscale tip as the spring in the classical model[23,27].

To gain insights into the observed discrete stick–slip process, MD simulations were carried out to simulate our experiments. As shown in Fig. 2a, the predicted lateral force (friction force)–displacement curve also exhibited two stick–slips (indicated by numbers 3–7) within one period of relative motion. The first force-drop (points 2–3) was found to be the force fluctuation induced by the interface structure relaxation (Fig. 2b,c and Extended Data Fig. 1). The lateral force reached the first stick point (point 4) and then dropped sharply after Slip1 (point 5 in Fig. 2a). The second stick–slip followed a similar routine (points 5–7 in Fig. 2a). Notably, the first slip did not lead to the dramatic drop of the lateral force, which was supposed to be attributed to the undulation of forces along other directions[6,22]. The slight deviations in the lateral force–displacement curve between the experiment and MD results (Figs. 1a and 2a) possibly resulted from the statistical discrepancy between the two-dimensional lattice measurement by TEM images and/or the algorithm for the average stress/force used in the MD simulation[28]. Sequential movement traces of interface atoms (deep-blue atoms, the top layer of the tip) are presented in Fig. 2b–h corresponding to points 1–7 in Fig. 2a. As shown in Fig. 2c–f, the interface atoms first shifted forwards along [110] and then some of them slipped into the hollow sites (indicated in Fig. 2j) along [11$\bar{1}$], while the rest stayed at their previous positions during slipping (Fig. 2c–f). For Slip 2, the majority of atoms moved further along [111] rather than [110] to complete the remaining movement of one period (Fig. 2g,h), implying a zigzag slipping pathway. This discrete stick–slip can be divided into two sliding events along two ⟨111⟩ directions to accomplish one entire period countermotion between asperities, consistent with the proposed pathway in two-dimensionally discrete friction[22,29,30] and dislocation-assisted slip[31]. Remarkably, we found the motion of atoms in the same layer was non-uniform in the simulation. For instance, the five atoms, indicated in different colours, showed different movement routes indicated by the circles in Fig. 2i. Compared to the red and grey atoms walking through one complete route (Fig. 2b–h), the black and yellow atoms just finished a half journey along the [11$\bar{1}$] or [111] directions (Fig. 2f–h). By contrast, the green atom only shifted a little near the initial position. The variety in the slipping pathways of these five atoms was in stark contrast to the uniform motion of the interface atoms predicted in the simulation of the Pt/Au system[30]. Our MD results further confirmed that the tip experienced a continuous elastic deformation, like a spring without severe plastic deformation (Extended Data Fig. 2). Additionally, the estimated friction coefficients from the experiment and MD were ~0.39 and ~0.21, respectively, comparable to the values reported in single-asperity stick–slip friction of, for example, copper (~0.8)[6] and MoS_2 (~0.2)[8]. The normal forces in the experiment and simulation are shown in Extended Data Figs. 3 and 1, respectively and the calculation is in Supplementary Discussion 2.

Similar results showing the discrete stick–slip friction have been found in the scenario with 11 contact atoms (Fig. 3 and Supplementary Video 2). As the tip slid almost 4.65 Å over one period, the shear force experienced two raise-drops, representing two separate slipping events. The asynchronous movement of interface atoms, as indicated by the yellow numbers in Fig. 3b–f, was consistent with the results shown in Fig. 1. The corresponding MD simulation verified similar phenomena with two stick–slips in one period (Extended Data Fig. 4a) and different sliding routes of the interface atoms (Extended Data Fig. 4b–i). However, it is worth noting that its slipping showed a higher friction force compared to the case in Figs. 1 and 2. For example, the detected maximum shear force and average friction force were 76.14 and 32.16 nN, respectively in the case with 11 contact atoms (Fig. 3), higher than those in the case with 7 contact atoms (Fig. 1). The difference of the friction force in these two cases should be ascribed to the differences in the contact area[21] and normal load[11]. An extra in situ friction experiment can be found in Supplementary Video 3.

Asynchronous accumulation and dissipation of strain energy

Furthermore, the dynamic evolution of lattice strain on the interface was surveyed as shown in Fig. 4. The shear strain on the top layer (layer 2, red atoms) was analysed by determining the position change of seven atoms (indicated by numbers 1–7) relative to the neighbouring layer (layer 1, blue atoms), as shown in Fig. 4a. Generally, the interface plane–strain distribution in friction is predicted by contact mechanics[32,33], or relies on indirect tools such as Raman spectra[34] for a rough estimation. Here, the accurate lattice strain could be directly measured from HRTEM images. The initial strain showed an inhomogeneous distribution with opposite shear strains, indicated by the red (positive) and blue (negative) arrows in Fig. 4a. As the friction went on, the accumulated elastic strain increased gradually (Fig. 4b,c) to a maximum value for activating the consequent slipping (Fig. 4d). All shear strain switched to positive and the distribution inhomogeneity in the magnitude and direction of strain was reduced (Fig. 4d). Then, the accumulated strain was only partly released after slipping and exhibited an inhomogeneous distribution again (Fig. 4e). This indicated that the accumulation and release of strain energy during friction are asynchronous and consistent with what is predicted by the modified Frenkel–Kontorova–Tomlinson (FKT) model[30], but in stark contrast to the uniform process described by the P–T model[27]. The shear strains measured from two selected atoms (atoms 1 and 7) confirmed this character, where the magnitude and direction of the shear strain for atom 1 differed from those for atom 7 during the friction process, and these two atoms displayed incompatible strain evolutions (Extended Data Fig. 5). The out-of-step movement of these two atoms was in accordance with the phenomenon shown in Fig. 2, implying the dynamic diversity of interface atoms.

To further verify the asynchronous accumulation and dissipation of strain energy, the stress evolution on the interface during the friction process was investigated using MD simulations. According to the force equilibrium between the substrate and tip during the friction process, the dynamic evolution of the shear stress field in the bottom layer of the substrate was analysed as shown in Fig. 5a–e. Here, the lateral shear stress is σ_{xy} and the vertical shear stress is

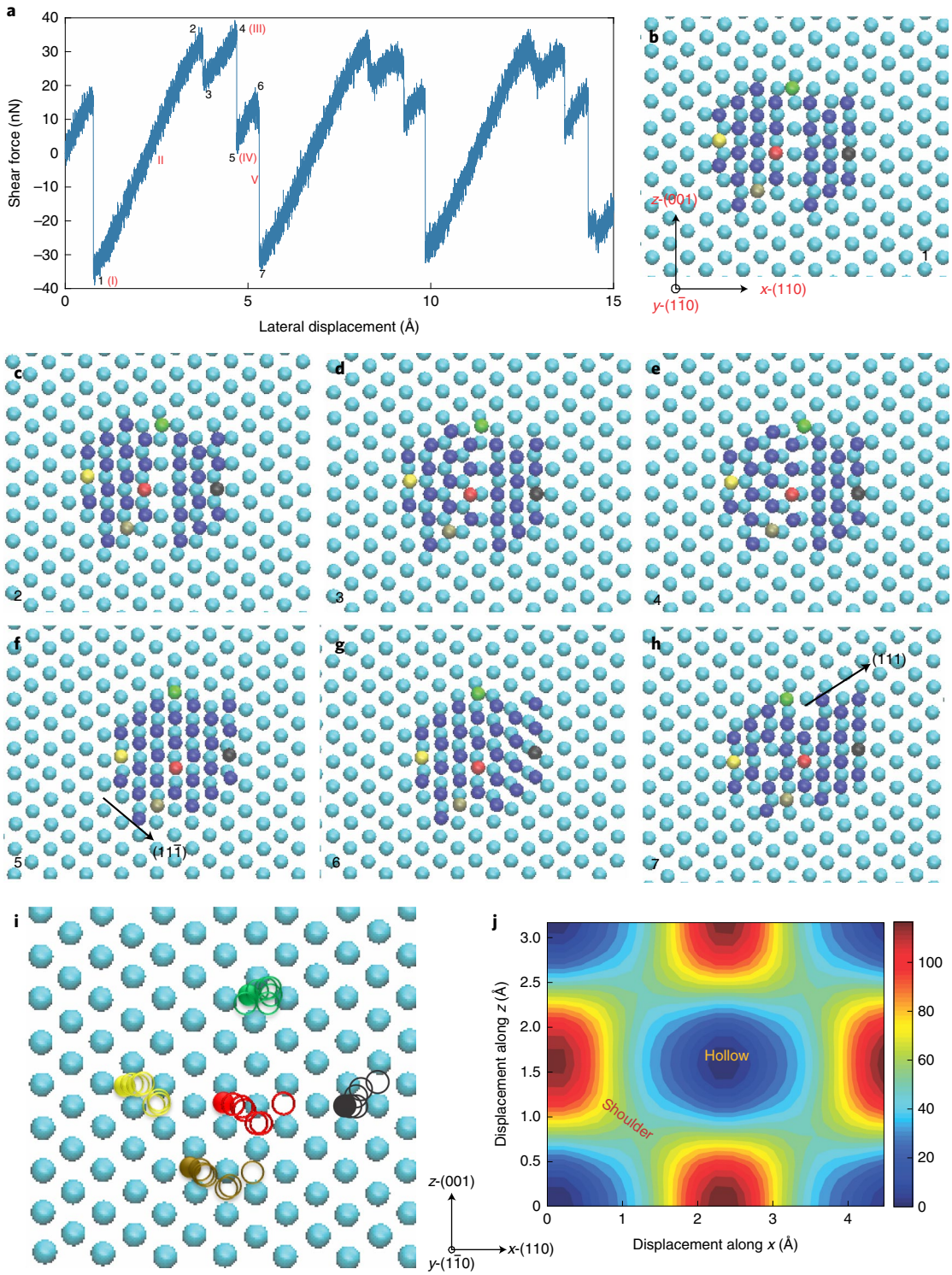

Fig. 2 | Discrete stick–slip behaviour between tungsten asperities revealed by MD simulations. a, Variation of the lateral force with the sliding displacement of the tip. **b**–**h**, Snapshots of the dynamic movement of atoms in the top layer of the tip with respect to the substrate. The bottom layer in the substrate (cyan atoms) served as the reference for the movement of atoms (deep blue) in the top layer of the tip. Some vacancies were included in the atomistic structure (**b**) used in our MD simulations (in MD methods). **i**, Motion traces of the selected five atoms, indicated by circles, within one friction period. The five selected atoms are coloured in yellow, green, red, black and grey, respectively in **b**–**i**. **j**, The interface potential landscape showing the potential variation with the interface structure. The red and blue regions correspond to the atom site and the hollow site, respectively. The lowest energy value in the landscape is set as zero. The color scale is in eV.

σ_{zy} and the corresponding sequences are indicated by the Roman numerals in Fig. 2a. Initially, σ_{xy} displayed a relatively homogeneous distribution with little area holding negative stress, compared to the inhomogeneous σ_{zy} field (Fig. 5a). As the friction progressed, the negative stress dominated the σ_{xy} field with the local region preserving high positive values while σ_{zy} experienced little change (Fig. 5b).

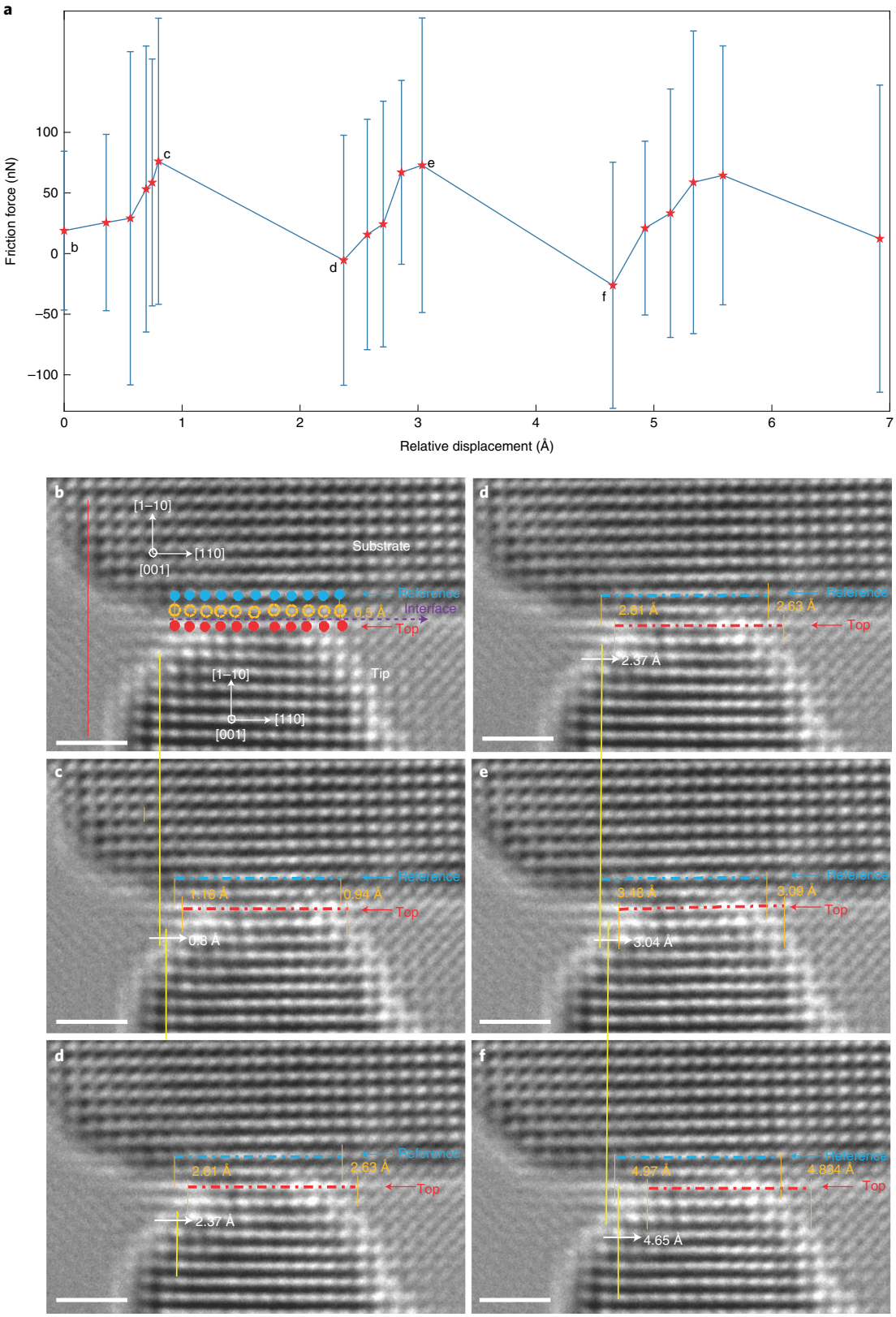

Fig. 3 | In situ TEM observation of atomic friction with 11 contact atoms. a, Variation of shear force with the sliding displacement of the tip. The error bars represent the standard deviation of the shear force. **b**–**f**, Serial images of the friction process at one period. The relative motion between asperities is indicated by the white arrows. The top layer of the tip and the reference layer of the substrate are indicated by the red and blue solid circles (in **b**) and short dotted lines (in **c**–**f**), respectively. The bottom layer in the substrate is indicated by broken circles. Two atom columns, indicated by the red and yellow vertical lines in the substrate and tip, respectively, served as the reference coordinates to determine the relative displacement between asperities. The absolute distance between the reference layer (substrate) and the interface layer (the top layer of the tip) along [110] is indicated by yellow numbers and the relative displacement between the substrate and the tip is indicated by white numbers. Scale bars, 1 nm. Panel **d** is repeated for ease of interpretation.

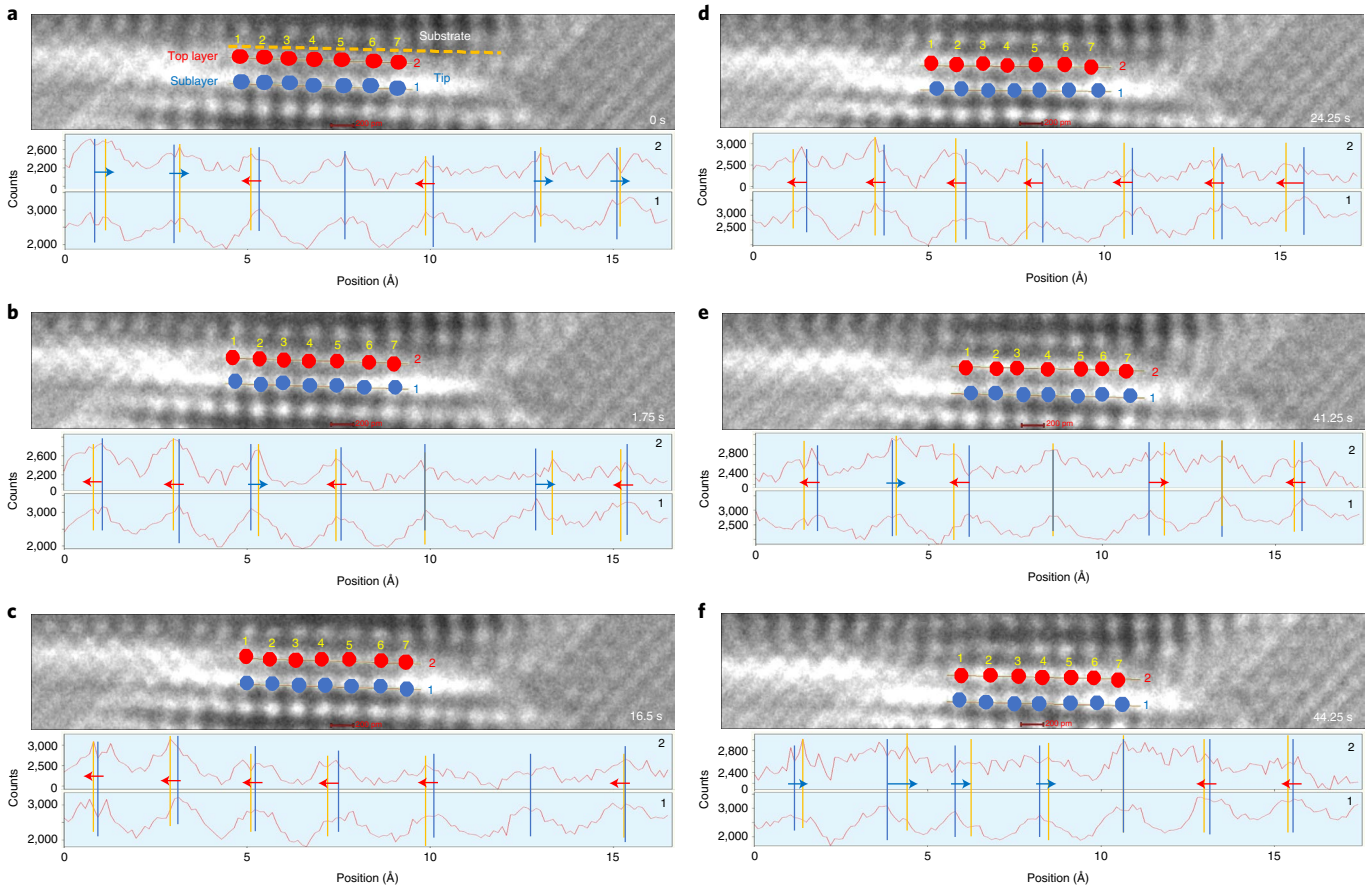

Fig. 4 | Strain evolution on the top layer of the tip during friction. a–f, Sequential images of the top layer during one friction period and the corresponding intensity profile. The selected top layer and the reference neighbouring sublayer are indicated with red lines 2 and 1, respectively. The atoms accounting for the strain are indicated by numbers 1–7. Geometric centres of atoms on the top layer and the reference neighbouring sublayer are indicated by orange and blue lines, respectively and the positive and negative shear strains are indicated by red and blue arrows, respectively.

Both σ_{xy} and σ_{zy} exhibited severely inhomogeneous distribution in the magnitude and direction of stress and such a high inhomogeneity in stress distribution is expected in incommensurate contacts[30]. Over the maximum point (III in Fig. 2a), σ_{xy} displayed a scattered distribution along [110], the countermotion direction, instead of disordered distribution as before (Fig. 5c). This implied that the atoms in the deep-blue region with high stress (Fig. 5c) would first slide followed by the motion of the rest of the atoms, showing the non-uniform movement of the interface atoms. This was consistent with our experimental results and the previous simulation results[22]. As the tip moved further, most accumulated σ_{xy} was released and it exhibited a strongly inhomogeneous distribution, whereas the σ_{zy} field displayed a relatively homogeneous distribution (Fig. 5d,e). The inhomogeneous stress distribution was also observed when using 11 contact atoms in the MD simulation. Both σ_{xy} and σ_{zy} experienced the transition from homogeneous to inhomogeneous distribution over one sliding period (Extended Data Fig. 6). Especially, they showed noticeably inhomogeneous stress distribution along the sliding direction after the second slipping (Extended Data Fig. 6e), which would possibly occur in friction hypothesized with multiple-dislocation-cooperated slip[35].

In situ HRTEM observation combined with MD simulation presented a dynamic picture of atomic discrete stick–slip friction in W single-asperity nanocontacts. The atomistic simulation implied that the nanoscale asperity tends to adopt a zigzag sliding route containing multiple steps with low energy barriers rather than a rigid slip along a given scanning direction, which is mainly attributed to the contact structure and sliding conditions between the asperities. For body-cubic centred (bcc) W, the easy-glide direction of dislocations is ⟨111⟩ in preference to ⟨110⟩[36], the preset scanning direction in friction. Furthermore, the atoms of the tip encounter the two-dimensional interaction potential landscape in contact (Fig. 2j) instead of the energy barrier along a single direction[27]. Another factor leading to discrete slipping is the alignment condition between the asperities[30]. As designed in our experiment, the substrate and the tip were aligned with a quite small misorientation, which allows us to image the contact of two asperities in a joint zone axis with atomic-scale resolution by TEM and avoids the incommensurate registry and the destruction of the surface potential periodicity[9,30]. The periodic symmetry of the interface potential with the diversity in sliding directions such as on the closely packed contact surface in face-cubic centred (fcc)[22,30], bcc and hexagonal-structured materials[5,26], gives rise to the discrete stick–slip. In addition, the scanning velocity of the tip (~0.01 nm s^{-1} used in the in situ experiments), which is even much lower than the sliding speed in AFM-based experiments (normally, several nanometres per second)[6], provided adequate time for the discrete stick–slip by allowing the atoms to move collectively to stable sites. This discrete stick–slip will lower the energy dissipation by increasing discontinuous stick points[22], whereas it is unlikely to occur in macro contacts due to the imperceptible pinning effect[22] and irregular asperity geometry[5].

Meanwhile, the convoluted surface potential and complex sliding pathway of the tip jointly raise the possibility that the movement of the atoms become inconsonant. The incommensurate contact

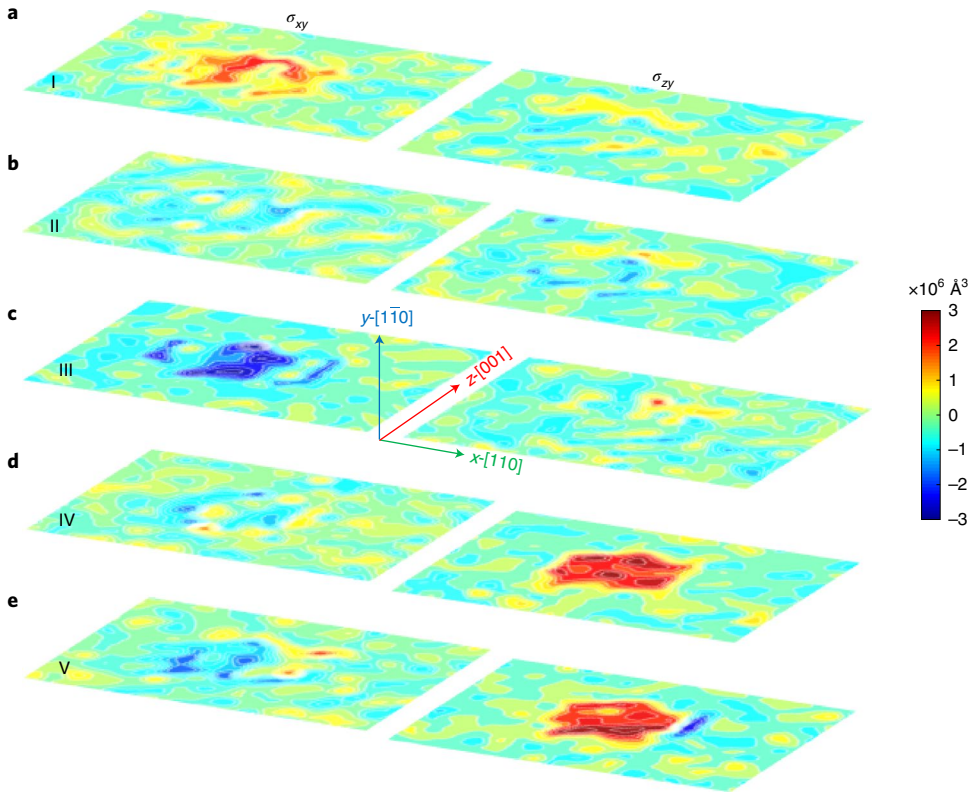

Fig. 5 | Dynamic evolution of shear stress field on the bottom layer of the substrate using MD simulation. a–e, Evolution of σ_{xy} (σ_{zy}) distribution on the bottom layer of the substrate. The corresponding sequences are indicated by the red Roman numerals in Fig. 2a. This virial stress is defined to account for the effects of momentum change of both mechanical forces and mass transport and has units of pressure × volume (bar × Å^3) where the volume is that of an individual atom[30].

by tailoring the orientation relationship between asperities[9,22,30] should contain a divided stress field with alternative negative and positive regions[30], suggesting that the strain incompatibility or the movement discordance of interface atoms plays a critical role in the magnitude change of the friction force and the transition between superlubricity and stick–slip. Implanting interface defects such as vacancies or interstitial atoms is believed to enhance the inhomogeneity of the surface structure and strain field[37]. In addition, presetting in-plane strain can be a practical approach to reduce the net friction force[34] by changing the surface or interaction potential corrugation. Nevertheless, it should be noted that the inhomogeneous in-plane stress field accompanied by atomic discreteness in flat contacts is different from the stress corrugation with the strain-induced atomic-scale roughness in models composed of the round tip–flat substrate couple[33,34]. Additionally, the hysteretic transmission of the strain/displacement within the nanoscale asperity regarded as a spring[27] may further facilitate the inhomogeneous stress distribution and non-uniform movement, which may directly cause energy dissipation by the irregular emission of phonons[38]. Notably, the friction between nanoscale W asperities did not exhibit the liquid-like or diffusion-mediated sliding reported in soft metal friction systems[12,14,39], which is attributed to the excellent thermal stability of W with the high cohesive energy[40] and high diffusion barriers[41,42] compared to Au and Ag[43]. In addition, the sliding velocity is ultralow (~0.1 nm s^{-1}), which contributes little to the sliding-induced heating rather than the linear friction welding[44].

In this study, two main sets of experiments and simulations were conducted with different contact areas as well as the cases with 7 and 11 contact atoms. Compared to the case with 7 contact atoms, the case with 11 contact atoms has ~2.35 times the contact area and more than 3 times the average normal load but shows ~1.98 times the average friction in the experiment. Notably, the contact area here was decided by the size of the sliding tip instead of depending on the normal load described in contact mechanics[45] and did not change appreciably in the whole friction process. This implies that the normal load might contribute in a limited way to the change of contact area in the atomically flat contact, compared to the classical tip-sample model (Figs. 1 and 3). The friction force only experienced a little change when the normal load dramatically decreased (Fig. 1a and Extended Data Fig. 3). The detected normal load also did not evolve periodically with the friction force as predicted by the simulation[22]. Admittedly, there existed uncertainty in the force measurement, which might hide the actual load dependency in friction. Nevertheless, these results still indicated that the contact area plays a more important role in deciding the magnitude of the friction force compared to the normal load[21,46]. Meanwhile, the low surface corrugation[33] and adhesive effect[21,47,48] between W asperities might make the friction force insensitive to the normal load. On account of the high vacuum under TEM, the passivation effect from adsorption on the W surface is limited. In contrast to the load-independence friction understood by thermolubricity in Krylov's model[49], our results showed a typical stick–slip with high friction rather than ultralow friction. Thus, the thermolubricity cannot explain the observed results here. Further studies are necessary to clarify the lack of load dependence of friction between single-asperity contacts. On the other hand, the design in atomic friction between the same crystals without misorientation here may be employed to estimate the ideal strength or lattice friction in the bulk crystal (Supplementary Discussion 3). It is worth noting that the shear strength obtained in our friction tests did not change appreciably as the normal load increased, indicating that the shear strength is not sensitive to the normal load but to the contact area.

Compared to the experimental results, the simulation results showed an extra force-drop in one sliding period (Fig. 2 and Extended Data Fig. 4). This extra force-drop is believed to result from the interface structure relaxation rather than a separate sliding (Fig. 2b,c and Supplementary Table 1). The high sliding speed (1 m s^{-1}) employed in the simulation indeed increases the possibilities of force fluctuations[22,50]. Moreover, compared to similar heights for two sticks in the experiment (Figs. 1a and 3a), the heights of the two peaks obtained from the MD simulations are quite different (Fig. 2a and Extended Data Fig. 4a). The second 'lower peak' in the simulation is supposed to be induced by the relaxation of the mechanical stress along the *z* direction (Extended Data Fig. 1), as observed in previous simulations[22,50]. However, this difference has rarely been captured in AFM-based experiments[5,26]. This implies that the high sliding speed in the simulations may be another plausible explanation for the second 'lower peak', by suppressing the fast force-drop. Bridging this speed gap[7] by employing advanced MD methods[50,51] could help reduce the difference between the experiments and the simulations. As the tip behaves like a spring (Extended Data Fig. 2), the displacement of the top layer lags behind the relative motion between two asperities causing the wider first stick phase compared to the second one in the simulations. This is hard to detect in experiments with ultralow sliding speed. In addition, the unreleased strain energy after the first slip may accelerate the second stick–slip process. Nevertheless, the experiments and MD simulations are in agreement about the discrete stick–slip atomic friction with non-uniform strain/stress distribution.

Conclusions

This work demonstrates a practical approach to visualizing the real-time friction at an atomic scale by designing single-asperity nanocontacts and performing controlled countermotion between asperities. Atomistic simulation revealed that the nanoscale tip adopts a zigzag pathway through two slipping steps along ⟨111⟩ to complete one full-period friction along ⟨110⟩ on the W {1$\bar{1}$0} contact surface. The accumulation and release of strain energy on the friction interface underwent an asynchronous evolution, accompanied by the inhomogeneous strain/stress distribution and a non-uniform movement of interface atoms during the friction process. These unique behaviours mainly resulted from the interface structure and sliding conditions of the asperities. Compared to the normal load, the contact area may play a more important role in atomic friction. The detailed motion trajectory and strain analysis of the interface atoms constructed an informative paradigm to clarify the dynamic diversity in real atomic friction, contributing to interpreting the friction mechanisms at the atomic scale.

Online content

Any methods, additional references, Nature Research reporting summaries, source data, extended data, supplementary information, acknowledgements, peer review information; details of author contributions and competing interests; and statements of data and code availability are available at https://doi.org/10.1038/s41565-022-01126-z.

Received: 24 December 2020; Accepted: 25 March 2022;
Published online: 23 May 2022

References

1. Achanta, S. & Celis, J.-P. in *Fundamentals of Friction and Wear on the Nanoscale* (eds Gnecco, E. & Meyer, E.) 631–656 (Springer, 2015).
2. Jacobs, T. D. B., Greiner, C., Wahl, K. J. & Carpick, R. W. Insights into tribology from in situ nanoscale experiments. *MRS Bull.* **44**, 478–486 (2019).
3. Park, J. Y. & Salmeron, M. Fundamental aspects of energy dissipation in friction. *Chem. Rev.* **114**, 677–711 (2014).
4. Mate, C. M., McClelland, G. M., Erlandsson, R. & Chiang, S. in *Scanning Tunneling Microscopy* (ed. Neddermeyer, H.) 226–229 (Springer, 1987).
5. Fujisawa, S. et al. The two-dimensional stick-slip phenomenon with atomic resolution. *Nanotechnology* **4**, 138–142 (1993).
6. Bennewitz, R. et al. Atomic-scale stick-slip processes on Cu(111). *Phys. Rev. B* **60**, R11301–R11304 (1999).
7. Liu, X.-Z. et al. Dynamics of atomic stick-slip friction examined with atomic force microscopy and atomistic simulations at overlapping speeds. *Phys. Rev. Lett.* **114**, 146102 (2015).
8. Lee, C. et al. Frictional characteristics of atomically thin sheets. *Science* **328**, 76–80 (2010).
9. Hirano, M., Shinjo, K., Kaneko, R. & Murata, Y. Anisotropy of frictional forces in muscovite mica. *Phys. Rev. Lett.* **67**, 2642–2645 (1991).
10. Li, Q., Dong, Y., Martini, A. & Carpick, R. W. Atomic friction modulation on the reconstructed Au (111) surface. *Tribol. Lett.* **43**, 369–378 (2011).
11. Socoliuc, A., Bennewitz, R., Gnecco, E. & Meyer, E. Transition from stick-slip to continuous sliding in atomic friction: entering a new regime of ultralow friction. *Phys. Rev. Lett.* **92**, 134301 (2004).
12. Merkle, A. P. & Marks, L. D. Liquid-like tribology of gold studied by in situ TEM. *Wear* **265**, 1864–1869 (2008).
13. Kizuka, T., Yamada, K., Deguchi, S., Naruse, M. & Tanaka, N. Cross-sectional time-resolved high-resolution transmission electron microscopy of atomic-scale contact and noncontact-type scannings on gold surfaces. *Phys. Rev. B* **55**, R7398–R7401 (1997).
14. Sato, T., Ishida, T., Jalabert, L. & Fujita, H. Real-time transmission electron microscope observation of nanofriction at a single Ag asperity. *Nanotechnology* **23**, 505701 (2012).
15. Oviedo, J. P. et al. In situ TEM characterization of shear-stress-induced interlayer sliding in the cross section view of molybdenum disulfide. *ACS Nano* **9**, 1543–1551 (2014).
16. Sato, T. et al. Real-time observation of slipping and rolling events in DLC wear nanoparticles. *Nanotechnology* **29**, 325707 (2018).
17. Jacobs, T. D. & Carpick, R. W. Nanoscale wear as a stress-assisted chemical reaction. *Nat. Nanotechnol.* **8**, 108–112 (2013).
18. Minor, A. M. & Dehm, G. Advances in in situ nanomechanical testing. *MRS Bull.* **44**, 438–442 (2019).
19. Wang, X. et al. Unstable twin in body-centered cubic tungsten nanocrystals. *Nat. Commun.* **11**, 2497 (2020).
20. Li, S. et al. The evolving quality of frictional contact with graphene. *Nature* **539**, 541–545 (2016).
21. Mo, Y., Turner, K. T. & Szlufarska, I. Friction laws at the nanoscale. *Nature* **457**, 1116–1119 (2009).
22. So, M., Jacobsen, K. W. & Stoltze, P. Simulations of atomic-scale sliding friction. *Phys. Rev. B* **53**, 2101–2113 (1996).
23. Dong, Y., Vadakkepatt, A. & Martini, A. Analytical models for atomic friction. *Tribol. Lett.* **44**, 367–386 (2011).
24. Sorensen, M. R., Brandbyge, M. & Jacobsen, K. W. Mechanical deformation of atomic-scale metallic contacts: Structure and mechanisms. *Phys. Rev. B* **57**, 3283–3294 (1998).
25. Zhong, L., Wang, J., Sheng, H., Zhang, Z. & Mao, S. X. Formation of monatomic metallic glasses through ultrafast liquid quenching. *Nature* **512**, 177–180 (2014).
26. Hölscher, H., Schwarz, U., Zwörner, O. & Wiesendanger, R. Consequences of the stick-slip movement for the scanning force microscopy imaging of graphite. *Phys. Rev. B* **57**, 2477–2481 (1998).
27. Hölscher, H., Schirmeisen, A. & Schwarz, U. D. Principles of atomic friction: from sticking atoms to superlubric sliding. *Phil. Trans. Roy. Soc. A* **366**, 1383–1404 (2008).
28. Subramaniyan, A. K. & Sun, C. Continuum interpretation of virial stress in molecular simulations. *Int. J. Solids Struct.* **45**, 4340–4346 (2008).
29. Fujisawa, S., Kishi, E., Sugawara, Y. & Morita, S. Two-dimensionally quantized friction observed with two-dimensional frictional force microscope. *Tribol. Lett.* **1**, 121–127 (1995).
30. Dong, Y., Li, Q., Wu, J. & Martini, A. Friction, slip and structural inhomogeneity of the buried interface. *Model. Simul. Mater. Sci. Eng.* **19**, 065003 (2011).
31. Hurtado, J. A. & Kim, K.-S. Scale effects in friction of single–asperity contacts. I. From concurrent slip to single–dislocation–assisted slip. *Proc. R. Soc. Lond. A* **455**, 3363–3384 (1999).
32. Maugis, D. Adhesion of spheres: the JKR-DMT transition using a Dugdale model. *J. Colloid Interface Sci.* **150**, 243–269 (1992).
33. Luan, B. & Robbins, M. O. The breakdown of continuum models for mechanical contacts. *Nature* **435**, 929–932 (2005).
34. Zhang, S. et al. Tuning friction to a superlubric state via in-plane straining. *Proc. Natl Acad. Sci. USA* **116**, 24452–24456 (2019).
35. Hurtado, J. A. & Kim, K.-S. Scale effects in friction of single–asperity contacts. II. Multiple–dislocation–cooperated slip. *Proc. R. Soc. Lond. A* **455**, 3385–3400 (1999).
36. Krenn, C. R., Roundy, D., Morris, J. W. Jr & Cohen, M. L. Ideal strengths of bcc metals. *Mater. Sci. Eng. A* **319**, 111–114 (2001).

37. Trevethan, T., Latham, C. D., Heggie, M. I., Briddon, P. R. & Rayson, M. J. Vacancy diffusion and coalescence in graphene directed by defect strain fields. *Nanoscale* **6**, 2978–2986 (2014).
38. Wang, Z.-J., Ma, T.-B., Hu, Y.-Z., Xu, L. & Wang, H. Energy dissipation of atomic-scale friction based on one-dimensional Prandtl-Tomlinson model. *Friction* **3**, 170–182 (2015).
39. Cross, G. et al. Adhesion interaction between atomically defined tip and sample. *Phys. Rev. Lett.* **80**, 4685–4688 (1998).
40. Bylander, D. & Kleinman, L. Self-consistent relativistic calculation of the energy bands and cohesive energy of W. *Phys. Rev. B* **29**, 1534–1539 (1984).
41. Ehrlich, G. & Stolt, K. Surface diffusion. *Annu. Rev. Phys. Chem.* **31**, 603–637 (1980).
42. Kim, S. Y., Lee, I.-H. & Jun, S. Transition-pathway models of atomic diffusion on fcc metal surfaces. I. Flat surfaces. *Phys. Rev. B* **76**, 245407 (2007).
43. Ambrosetti, A. & Silvestrelli, P. L. Cohesive properties of noble metals by van der Waals-corrected density functional theory: Au, Ag, and Cu as case studies. *Phys. Rev. B* **94**, 045124 (2016).
44. Vairis, A. & Frost, M. High frequency linear friction welding of a titanium alloy. *Wear* **217**, 117–131 (1998).
45. Schwarz, U. D. A generalized analytical model for the elastic deformation of an adhesive contact between a sphere and a flat surface. *J. Colloid Interface Sci.* **261**, 99–106 (2003).
46. Gao, G., Cannara, R. J., Carpick, R. W. & Harrison, J. A. Atomic-scale friction on diamond: a comparison of different sliding directions on (001) and (111) surfaces using MD and AFM. *Langmuir* **23**, 5394–5405 (2007).
47. Ruths, M., Alcantar, N. & Israelachvili, J. Boundary friction of aromatic silane self-assembled monolayers measured with the surface forces apparatus and friction force microscopy. *J. Phys. Chem. B* **107**, 11149–11157 (2003).
48. Gosvami, N. N., Filleter, T., Egberts, P. & Bennewitz, R. Microscopic friction studies on metal surfaces. *Tribol. Lett.* **39**, 19–24 (2010).
49. Krylov, S. Y. & Frenken, J. W. Thermal contact delocalization in atomic scale friction: a multitude of friction regimes. *New J. Phys.* **9**, 398 (2007).
50. Dong, Y., Li, Q. & Martini, A. Molecular dynamics simulation of atomic friction: A review and guide. *J. Vac Sci. Technol. A* **31**, 030801 (2013).
51. Li, J. et al. Diffusive molecular dynamics and its application to nanoindentation and sintering. *Phys. Rev. B* **84**, 054103 (2011).

Methods

Probe and substrate preparation. W rods (99.97 wt% purity, 0.13-inch diameter) purchased from ESPI Metals were chemically etched. In the experimental set-up, multiple nanoteeth of a fractured surface in a cut-off W rod[52] with desired orientations served as the stiff substrate (Supplementary Fig. 1) and one electrochemically etched W tip acted as the mobile asperity (Supplementary Figs. 2 and 3). A bulk W rod was fractured to obtain numerous nanosized tips and one nanosized crystal with a [001] zone axis was selected as the asperity candidate in the in situ TEM experiments. A bias was applied between the selected nanocrystal (the asperity as the substrate) surface and the prepared W probe (the asperity as the mobile tip) after making them contact and the substrate and the tip would weld together due to the Joule heating. These two asperities, the sample-side substrate and the probe-side tip, slid with each other and were then separated by controlling the lateral and longitudinal movement of the probe, driven by a scanning transmission microscope-holder piezo system. The contact, welding, slide and separation process was repeated to obtain the final substrate and tip with a perfectly smooth surface. The lattice constant of tungsten is 3.16 Å and its melting point is ~3,422 °C. The comparable stiffness between the tip and substrate (which are made of the same materials) could effectively prevent the severe deformation of one asperity.

In situ experiments. The finite top area of the W tip prepared was on purpose smaller than that of the substrate to allow the countermotion to be conducted conveniently. By further precisely tuning the separation distance and the alignment between the tip and the substrate, the nanocontact was acquired to form the friction pair (Supplementary Video 4). The W tip with a smooth top surface was controlled to approach the substrate bottom through the piezo system. The friction was carried out by driving the lateral motion of the W tip and the scanning velocity was controlled by the tip motion step (~0.004 nm). Thus, the atomic-friction process was visualized during a controlled countermotion between the two tungsten asperities. The real-time friction was captured by the continuous imaging snapshots (4 frames per second) of the software TIA provided by FEI under the observation of aberration correction transmission electron microscopy using an FEI Titan Themis G2 200 instrument at 200 kV with a high vacuum value of $\leq 2\times10^{-7}$ Torr. The screen current density is 2×10^{3}–10^{4} e $A^{-2}s^{-1}$. The excellent thermal stability of the W sample depresses the radiation effect from the electron beam during TEM imaging and a high vacuum environment alleviates the existence of interfacial contamination. The measurement of the lattice strain/stress from HRTEM images (Supplementary Fig. 4) performed using TIA provides an effective method to estimate the shear and compression forces[53], avoiding the complex calibration for lateral force required in AFM-based technology[54].

MD simulations. The atomistic MD simulations were performed using the LAMMPS code[55]. The interatomic potential within the embedded atom method (EAM)[56] formalism was employed in the simulations[57]. All the MD simulations were performed in the canonical ensemble. The temperature of the system was set at 300 K by applying a Nosé–Hoover thermostat[58]. The equation of motion was integrated using the velocity Verlet algorithm with a time step of 1 fs. The probe was modelled with a truncated cone-shaped slab consisting of 1,242 atoms (for the case of 11 contact atoms in Extended Data Fig. 4 the probe contained 1,467 atoms) and the substrate was modelled with a rectangular-shaped slab consisting of 4,666 atoms in Fig. 2. Several vacancies were introduced to the top surface of the probe to ensure the friction event occurred at the interface, otherwise the shear would happen within the 2–3 layers of atoms in the probe-side crystal away from the interface. The positions of the atoms at the boundary zone containing three atom layers were fixed whereas all the other atoms were allowed to move. During the MD simulations, non-periodic boundary conditions were assumed along all dimensions. The friction process was modelled in two stages: (1) the W probe first approached the substrate at a speed of 0.01 nm ps^{-1} in the direction normal to the surface. After every 0.025 nm step, the system was subjected to a 15 ps equilibration to relax the structure; (2) at a desired vertical distance between the probe and the substrate, the probe slid parallelly at a controlled speed of 1 m s^{-1}. The force, virial stress between the probe and the substrate and the resulting structures were extracted for further analysis. In addition, the interface potential landscape at the given separation distance between the probe and substrate was plotted by evaluating the system energy after rigidly shifting the probe along the vectors parallel to the friction plane. During the simulation, only the positions of the atoms along the normal direction of the interface were allowed to relax.

Data availability

All data needed to evaluate the conclusions have been included in the paper/or the Supplementary Materials. Source data are provided with this paper. Additional data related to this paper can be requested from the corresponding authors S.X.M. (sxm2@pitt.edu) or G.W. (guw8@pitt.edu).

References

52. Wang, J. et al. Discrete shear band plasticity through dislocation activities in body-centered cubic tungsten nanowires. *Sci. Rep.* **8**, 4574 (2018).
53. Sun, S. et al. Atomistic mechanism of stress-induced combined slip and diffusion in sub-5 nanometer-sized Ag nanowires. *ACS Nano* **13**, 8708–8716 (2019).
54. Liu, E., Blanpain, B. & Celis, J.P. Calibration procedures for frictional measurements with a lateral force microscope. *Wear* **192**, 141–150 (1996).
55. Plimpton, S. Fast parallel algorithms for short-range molecular dynamics. *J. Comput. Phys.* **117**, 1–19 (1995).
56. Daw, M. S. & Baskes, M. I. Embedded-atom method: Derivation and application to impurities, surfaces, and other defects in metals. *Phys. Rev. B* **29**, 6443–6453 (1984).
57. Ding, Z., Zhou, S. & Zhao, Y. Hardness and fracture toughness of brittle materials: a density functional theory study. *Phys. Rev. B* **70**, 184117 (2004).
58. Hoover, W. G. Canonical dynamics: Equilibrium phase-space distributions. *Phys. Rev. A* **31**, 1695–1697 (1985).

Acknowledgements

S.X.M. acknowledges support from the National Science Foundation (NSF CMMI 1824816) through the University of Pittsburgh. G.W. acknowledges the computational resources provided by the University of Pittsburgh Center for Research Computing.

Author contributions

S.X.M. conceived the project. X.W. designed the experiment and performed in situ TEM tests and associated result analysis. Y.H. contributed to the experiment design and the result discussion. S.T. contributed to the TEM observation. Z.L. and G.W. carried out MD simulations. X.W., Z.L., G.W. and S.X.M. wrote the manuscript with the contribution of all authors.

Competing interests

The authors declare no competing interests.

Additional information

Extended data is available for this paper at https://doi.org/10.1038/s41565-022-01126-z.

Supplementary information The online version contains supplementary material available at https://doi.org/10.1038/s41565-022-01126-z.

Correspondence and requests for materials should be addressed to Guofeng Wang or Scott X. Mao.

Peer review information *Nature Nanotechnology* thanks the anonymous reviewers for their contribution to the peer review of this work.

Reprints and permissions information is available at www.nature.com/reprints.

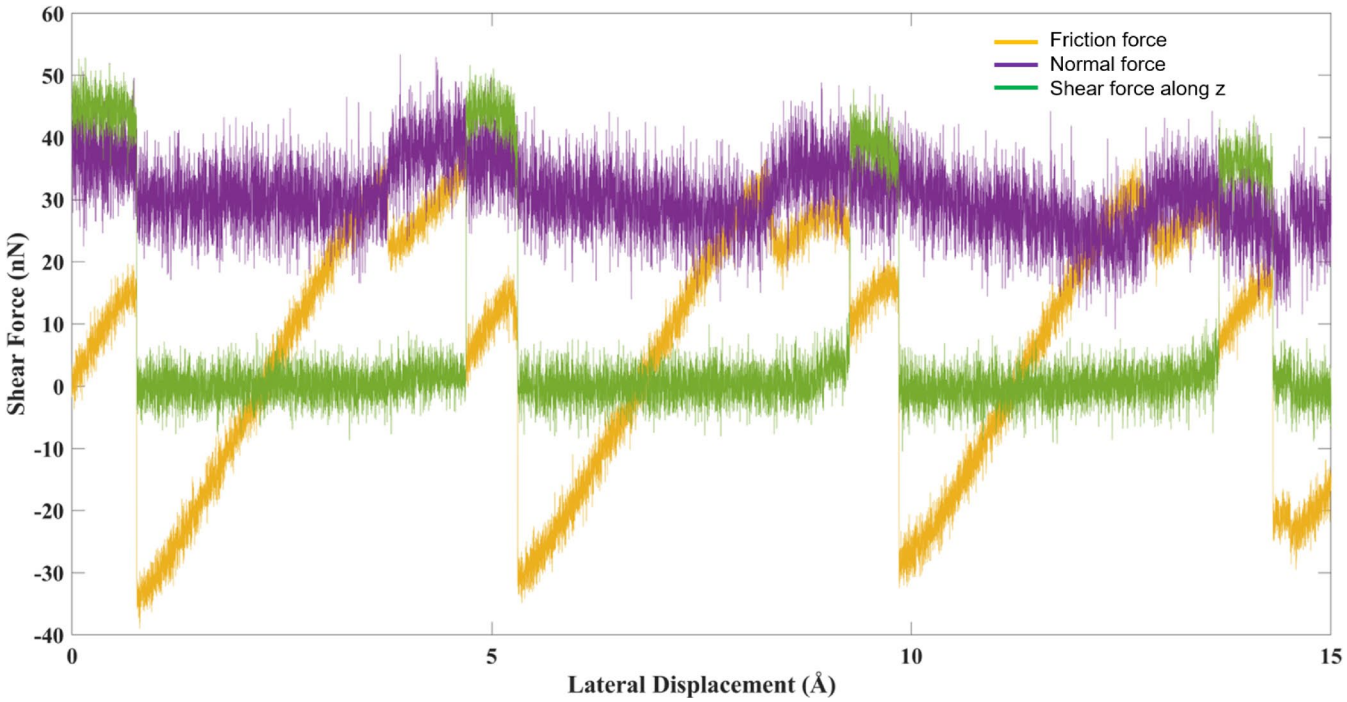

Extended Data Fig. 1 | Three force components of the interface atoms in MD simulation with 7 contact atoms. (Fig. 2) When the interface atoms completed the second slipping along the zig-zag route, the accumulated stress along z-direction in the first slipping would release, leading to the drop of the friction force. In experiments, since the shear force was obtained by measuring shear strains of seven/eleven atoms along x-direction in contact, the effect from the stress release along z-direction on the friction force might not be noticed.

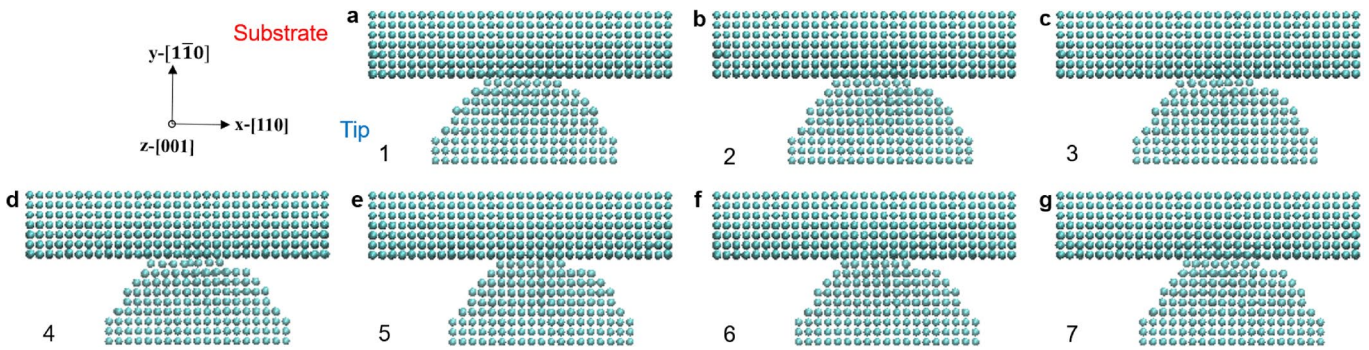

Extended Data Fig. 2 | The friction process within one period in MD simulation. (a-g) The structure evolution of the single asperity W-W contacts during friction, corresponding to the points of numbers 1–7 in Fig. 2a.

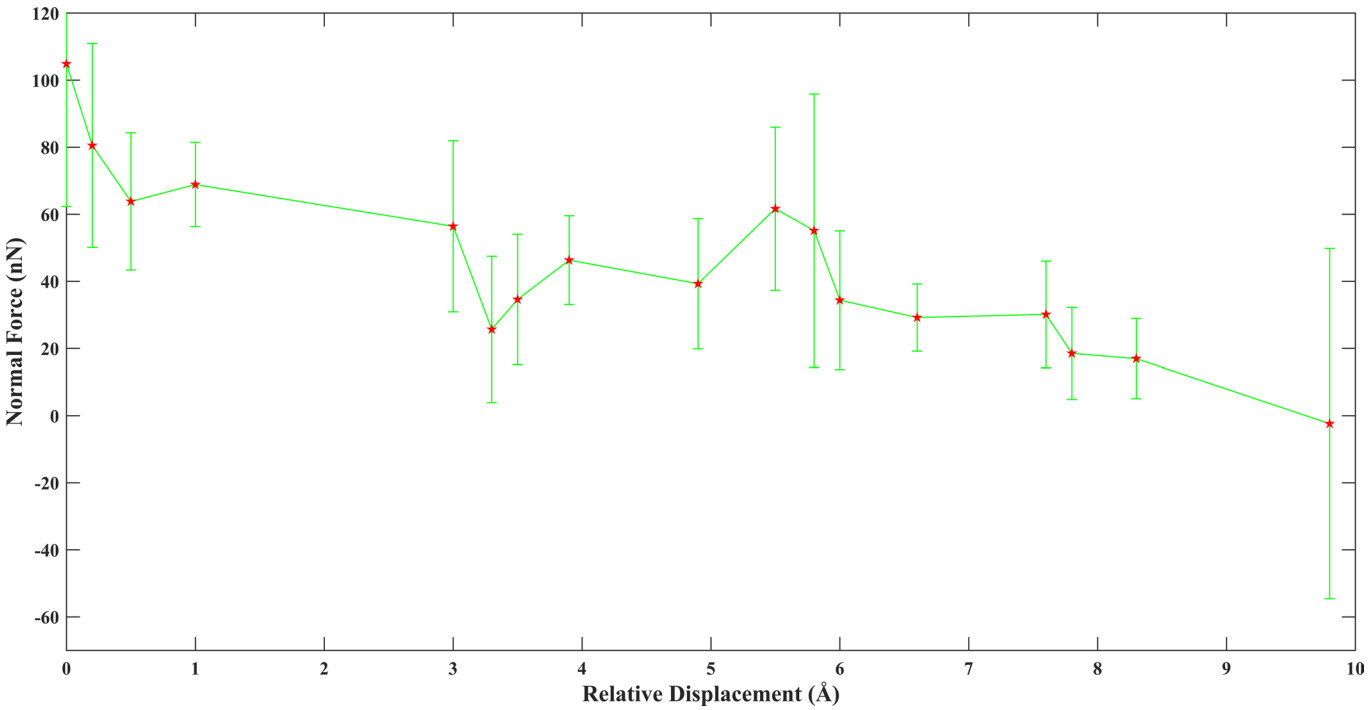

Extended Data Fig. 3 | Variation of normal force with the displacement of the tip in the experiment (Fig. 1). The error bars represent the standard deviation of the normal force.

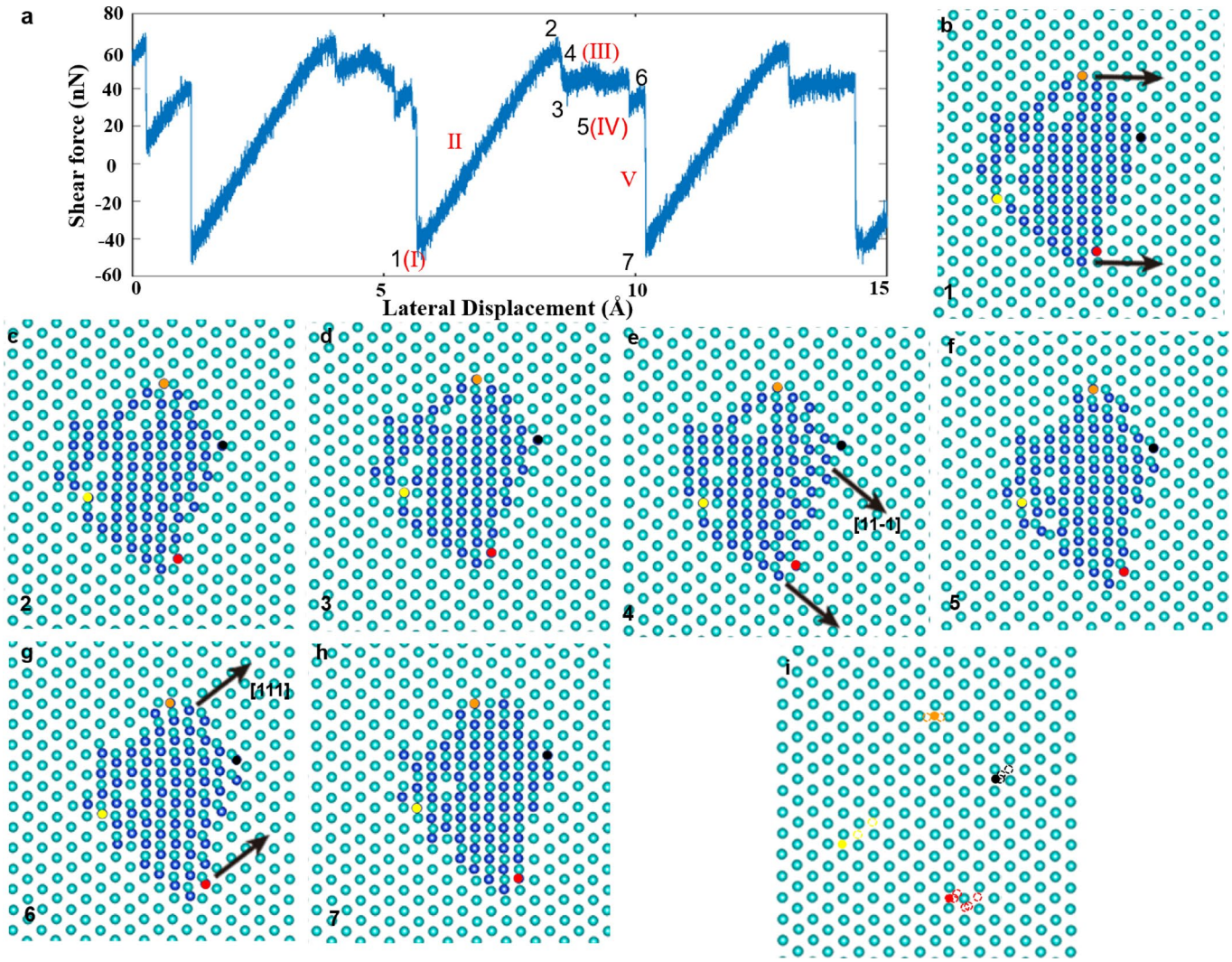

Extended Data Fig. 4 | Discrete stick-slip behavior between tungsten asperities revealed by molecular dynamics (MD) simulation (The width of the contact region is 11 atoms' space). (a) The function of the lateral force with the sliding displacement of the tip. (b-h) The snapshots of the dynamic movement of atoms in the top layer of the tip with respect to the substrate. The cyan balls represent the atoms in the bottom of the substrate. Four selected atoms were colored in yellow, orange, red, dark respectively. (i) The motion traces of the selected four atoms marked by the broken circles within one friction period.

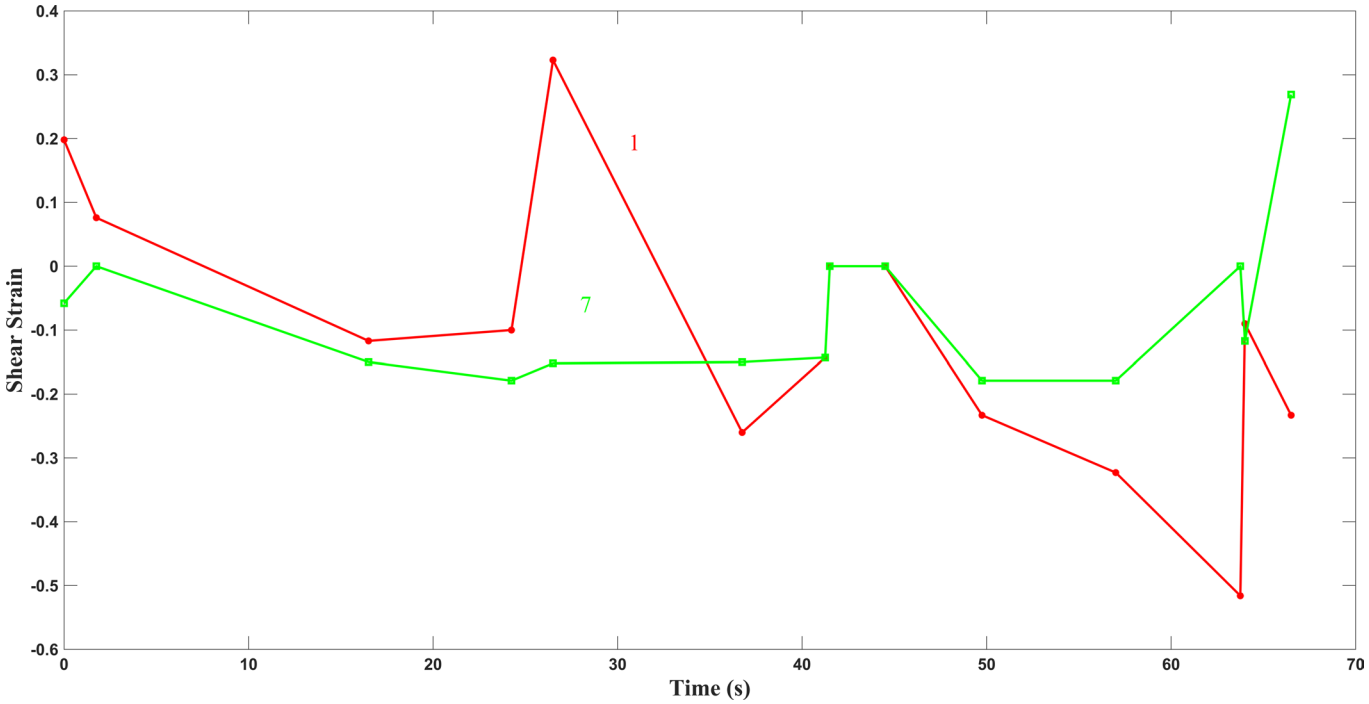

Extended Data Fig. 5 | The shear strain evolutions measured from two selected atoms marked by 1 and 7 in Fig. 4 during friction within one period.

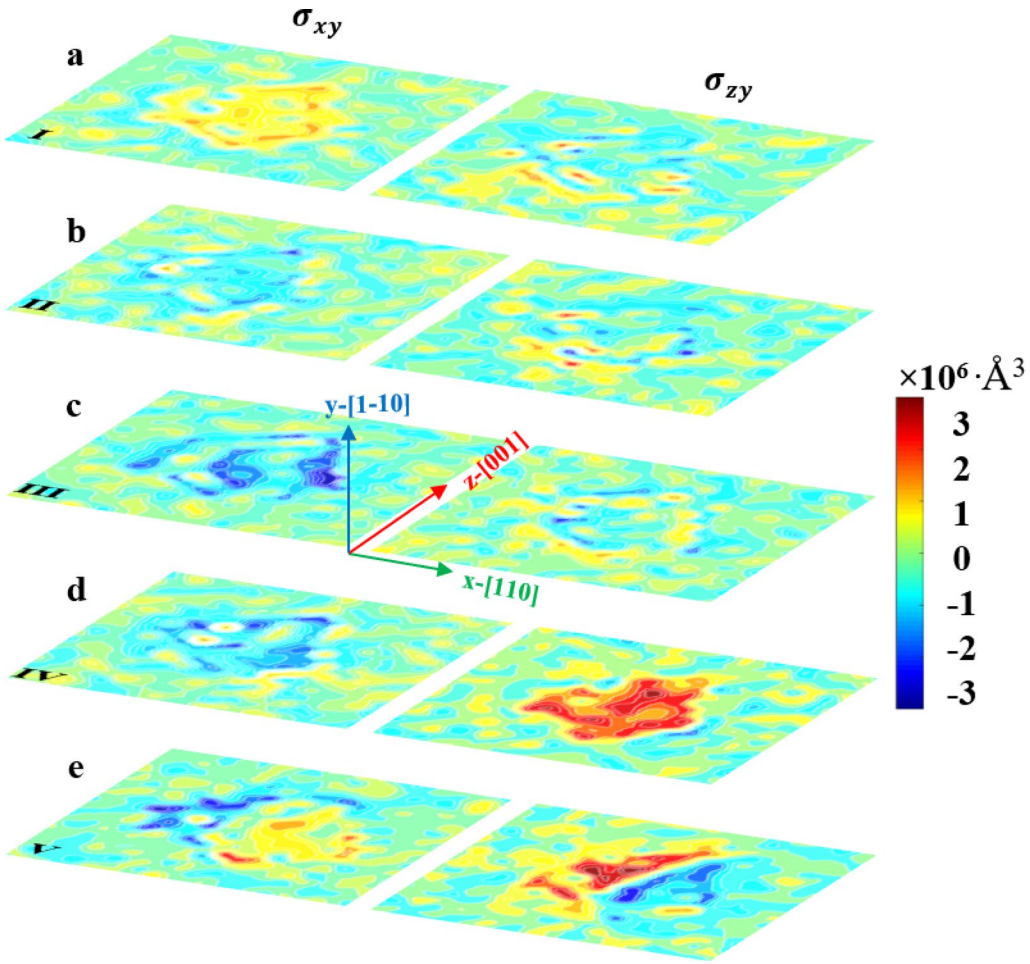

Extended Data Fig. 6 | Dynamic evolution of shear stress field on the bottom layer of the substrate in MD simulation. (a-e) The evolution of σ_{xy} (σ_{zy}) distribution on the bottom layer of the substrate and the corresponding sequences are indicated by red Roman numbers in Extended Data Fig. 4a.

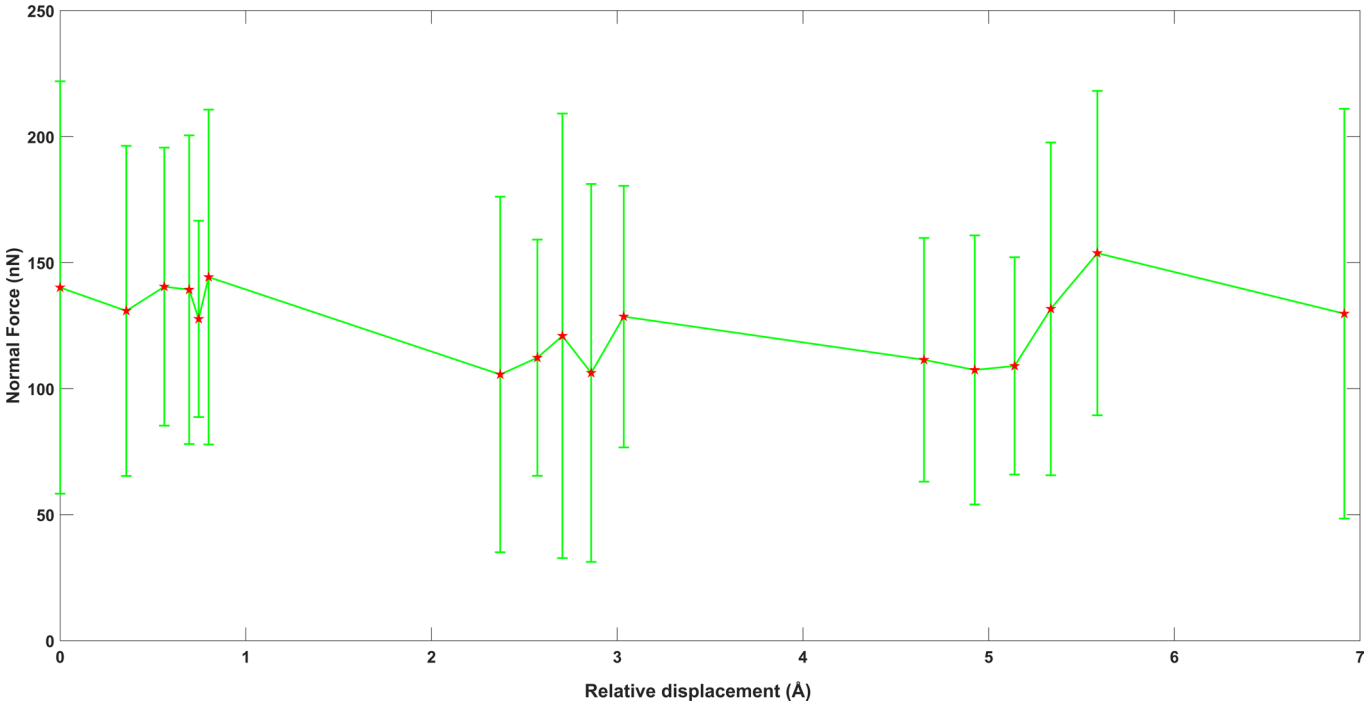

Extended Data Fig. 7 | Variation of normal force with the displacement of the tip in the case with 11 contact atoms. The error bars represent the standard deviation of the normal force.